Pulsations in the atmosphere of the rapidly oscillating Ap star 10 Aquilae[★]

M. Sachkov,[1]† O. Kochukhov,[2] T. Ryabchikova,[1,3] D. Huber,[3] F. Leone,[4] S. Bagnulo[5] and W. W. Weiss[3]

[1]*Institute of Astronomy, Russian Academy of Sciences, Pyatnitskaya 48, 119017 Moscow, Russia*
[2]*Department of Physics and Astronomy, Uppsala University Box 515, SE-751 20 Uppsala, Sweden*
[3]*Department of Astronomy, University of Vienna, Türkenschanzstrasse 17, A-1180 Wien, Austria*
[4]*Dipartimento di Fisica ed Astronomia, Universitá di Catania, via S. Sofia 78, 95123 Catania, Italy*
[5]*Armagh Observatory, College Hill, Armagh BT61 9DG*

ABSTRACT

The rapidly oscillating Ap (roAp) star 10 Aquilae (10 Aql) shows one of the lowest photometric pulsation amplitudes and is characterized by an unusual spectroscopic pulsational behaviour compared to other roAp stars. In summer 2006 this star became target of an intense observing campaign, that combined ground-based spectroscopy with space photometry obtained with the MOST (Microvariability & Oscillations Stars) satellite. More than 1000 spectra were taken during seven nights over a time-span of 21 d with high-resolution spectrographs at the 8-m European Southern Observatory (ESO) Very Large Telescope (VLT) and 3.6-m Telescopio Nazionale Galileo (TNG) giving access to radial velocity variations of about 150 lines from different chemical species. A comparison of pulsation signatures in lines formed at different atmospheric heights allowed us to resolve the vertical structure of individual pulsation modes in 10 Aql which is the first time for a multiperiodic roAp star. Taking advantage of the clear oscillation patterns seen in a number of rare earth ions and using the contemporaneous MOST photometry to resolve aliasing in the radial velocity measurements, we improve also the determination of pulsation frequencies. The inferred propagation of pulsation waves in 10 Aql is qualitatively similar to other roAp stars: pulsation amplitudes become measurable in the layers where Y and Eu are concentrated, increase in layers where the Hα core is formed, reach a maximum of 200–300 m s^{-1} in the layers probed by Ce, Sm, Dy lines and then decrease to 20–50 m s^{-1} in the layers where Nd III and Pr III lines are formed. A unique pulsation feature of 10 Aql is a second pulsation maximum indicated by Tb III lines which form in the uppermost atmospheric layers and oscillate with amplitudes of up to 350 m s^{-1}. The dramatic decline of pulsations in the atmospheric layers probed by the strong Pr III and Nd III lines accounts for the apparent peculiarity of 10 Aql when compared to other roAp stars. The phase–amplitude diagrams and bisector measurements of the Nd III 5102 Å line reveal a rapid change of phase and amplitude with height for all three main pulsation modes, indicating the presence of a pulsation node in the stellar atmosphere. Finally, we report the discovery of a puzzling asymmetry of the strong Nd III lines with their blue wing extending up to -50 km s^{-1}, which is about 25 times the estimated value of $v_e \sin i$.

Key words: stars: atmospheres – stars: chemically peculiar – stars: individual: 10 Aql – stars: magnetic fields – stars: oscillations.

1 INTRODUCTION

More than 30 members among the group of late A magnetic chemically peculiar stars exhibit high-overtone, low-degree, non-radial *p*-mode pulsations with periods in the range of 6–21 min (Kurtz & Martinez 2000). These *rapidly oscillating Ap* (roAp) stars are characterized by strong global magnetic fields with a polar strength

of the order of 1–10 kG. The atmospheres of roAp stars are enriched with heavy elements, brought up from the stellar interior by diffusion. Conspicuous lateral and vertical variations of chemical abundances in Ap stars and the prominence of the magnetic field signatures make them primary targets for detailed investigations of the magnetic topology and magnetically driven formation of structures in stellar atmospheres (Kochukhov 2004a; Ryabchikova 2004).

The observed pulsational amplitudes of roAp stars are modulated according to the visible magnetic field structure. This observation led to the oblique pulsator model (Kurtz 1982), where axisymmetric $\ell = 1$ modes are aligned with the magnetic field axis, which itself is oblique to the axis of stellar rotation. Calculations by Saio & Gautschy (2004) showed that dipolar modes are significantly distorted by a magnetic field of kG strength, but retain their axisymmetric character. On the other hand, the structure of pulsational perturbations can include significant non-axisymmetric components in weak-field stars (Bigot & Dziembowski 2002). The indirect pulsation Doppler imaging of oscillations in the prototype roAp stars HR 3831 (Kochukhov 2004b) vindicated the oblique pulsator model and for the first time characterized observationally the magnetic distortion of the global *p*-modes.

The roAp stars are key objects for asteroseismology, which presently is the most powerful tool for testing theories of stellar structure and evolution. The classical asteroseismic analysis, utilizing precise frequency measurements, helps to constrain the luminosity and internal chemical composition of pulsating magnetic stars (e.g. Matthews, Kurtz & Martinez 1999; Cunha, Fernandes & Monteiro 2003). Recent time-resolved spectroscopic observations of roAp stars utilizing large telescopes (see review by Kochukhov 2007a) demonstrated the possibility of another type of asteroseismic investigation, which is focused on the upper atmospheric layers. A significant chemical stratification and a short vertical wavelength of pulsation modes lead to a remarkable diversity of the pulsational characteristics observed in individual spectral lines, notably of absorption lines of the rare earth elements (REEs; e.g. Kochukhov & Ryabchikova 2001a; Mkrtichian, Hatzes & Kanaan 2003; Ryabchikova et al. 2007a). The information extracted from the lines formed at different optical depths opens access to different modes and can be combined to yield a vertical tomographic map of the pulsating stellar atmosphere (Ryabchikova et al. 2007b). Thus, applying Doppler imaging techniques and pulsation tomography to line profile variation in roAp stars promises an unprecedented three-dimensional (3D) picture of magnetoacoustic pulsations (Kochukhov 2005).

These spectacular results have been obtained despite the fact that most spectroscopic observations of roAp stars were obtained in a snapshot mode and hence cover only a few hours of stellar oscillations. A detailed frequency analysis is highly ambiguous with such limited data, because of the well-known aliasing problem. It can only marginally improved by combining observations from several nights, but which rarely are available when large telescopes had to be used. Therefore, despite an outstanding clarity of the pulsation curves often produced with spectroscopy, for most multiperiodic roAp stars they correspond to an unresolved mixture of different modes and thus are exceedingly difficult to interpret. This fundamental problem can be alleviated by simultaneous photometric observations with a high duty cycle, as it was successfully demonstrated by a combination of space photometry of the roAp star HD 24712 with contemporaneous Very Large Telescope/UV–Visual Echelle Spectrograph (VLT/UVES) spectroscopy (Ryabchikova et al. 2007a). In this paper we present

an analysis of a much more extensive spectroscopic time series for another pulsating Ap star, 10 Aquilae (10 Aql), which was observed simultaneously from ground and space.

10 Aql (HR 7167, HD 176232, HIP 93179) is one of the brightest roAp stars. Ryabchikova et al. (2000) performed its model atmosphere and abundance analysis using high-resolution spectra. They have estimated $T_{\text{eff}} = 7550$ K, $\log g = 4.0$, and derived $M = 2.0 \pm 0.2 \, M_{\odot}, R = 2.5 \pm 0.2 \, R_{\odot}$ from the comparison of the stellar parameters with theoretical evolutionary tracks. Kochukhov & Bagnulo (2006) have included 10 Aql in their study of the evolutionary state of magnetic chemically peculiar stars. Adopting a photometric temperature $T_{\text{eff}} = 7900$ K, they found $M = 1.95 \pm 0.04 \, M_{\odot}, \log L = 1.32 \pm 0.05$ and a fractional age of 64–76 per cent of the main-sequence lifetime. The abundance pattern of 10 Aql is characteristic of a cool Ap star. A notable spectral anomaly is the overabundance of the doubly ionized REEs, Pr III and Nd III.

A longitudinal magnetic field of about 500 G was detected in 10 Aql by Babcock (1958), Preston (1970) and Ryabchikova et al. (2005). Using magnetic Zeeman splitting in unpolarized spectra Kochukhov et al. (2002) provided the first measurement of the mean magnetic field modulus in 10 Aql, $\langle B \rangle = 1.5 \pm 0.1$ kG, which later was confirmed by Leone, Vacca & Stift (2003), and they estimated the projected rotational velocity $v_e \sin i = 2.0 \, \text{km s}^{-1}$. The sharpness of spectral lines and the absence of measurable variations of the mean longitudinal magnetic field indicate that 10 Aql has a long rotational period.

Recently, Ryabchikova, Kochukhov & Bagnulo (2008) have studied the vertical stratification and isotope anomaly of Ca in a number of Ap stars, including 10 Aql. These authors found a concentration of Ca in deeper atmospheric layers and invoked a vertical separation of the Ca isotopes to explain the shape of the Ca II infrared triplet lines. A comprehensive chemical stratification analysis of 10 Aql is currently underway by Nesvacil et al. (in preparation), but already a preliminary result (Nesvacil, Weiss & Kochukhov 2008) shows that Si, Ca, Cr, Fe and Sr share a qualitatively similar vertical abundance distribution, characterized by a rapid increase of the element abundances below $\log \tau_{5000} \approx -1$. A redetermination of the atmospheric parameters taking into account individual chemical abundances and stratification supports the spectroscopic $T_{\text{eff}} \approx 7600$ K obtained by Ryabchikova et al. (2000).

Photometric variations with a period close to 11.4 min and an amplitude below 0.5 mmag were discovered in 10 Aql by Heller & Kramer (1988). Heller & Kramer (1990) identified three pulsation modes with periods of 11.06–13.45 min, based on 26 h of high-speed photometry in the *B* band. Despite an aliasing problem in their data, Heller & Kramer (1990) were able to determine the large frequency separation, $\Delta \nu = 50.6 \, \mu$Hz. Belmonte, Martinez Roger & Roca Cortes (1991) collected 47 h of time-resolved photometry in the *J* band, confirming oscillations in 10 Aql. Moreover, their study suggested that the amplitude of the infrared photometric variations significantly exceeds variations in the *B* band, which is unusual for a roAp star (e.g. Martinez, Sekiguchi & Hashimoto 1994; Matthews et al. 1996). However, no oscillations were detected in the follow-up photometric monitoring conducted in the *H* band (Belmonte, Kreidl & Martinez Roger 1992).

Radial velocity (RV) variations with previously known oscillation periods were discovered in 10 Aql by Kochukhov et al. (2002). Over two nights they observed the star during a total of 8 h in a short-wavelength region centred at λ6150 Å. Unlike the majority of other roAp stars, 10 Aql showed only a weak variability with an amplitude of $\approx 30 \, \text{m s}^{-1}$ in the strong Nd III 6145 Å line, but exhibited amplitudes at the level of 80–130 m s^{-1} in the lines of

Table 1. Pulsation frequencies of 10 Aql identified in the MOST photometric campaign (Huber et al. 2008). The numbers in brackets give the estimated error in units of the last significant digit. The two candidate frequencies, f_i and f_j, are possibly present in the MOST data but could not be definitely confirmed.

Id	ν (mHz)	P (min)	A (mmag)
f_1	1.44 786(3)	11.5112(2)	0.17(1)
f_2	1.39 691(3)	11.9311(3)	0.15(1)
f_3	1.42 709(4)	11.6788(3)	0.12(1)
f_i	1.3 662(1)	12.199(1)	0.03(2)
f_j	1.4 686(1)	11.349(1)	0.03(2)

first REE ions, Gd II and Eu II. Aiming to extend the study of pulsational variation of 10 Aql, Hatzes & Mkrtichian (2005) analysed spectra covering 11.6 h of time-resolved observations during three nights. Somewhat surprisingly, despite a broad wavelength coverage of their data, Hatzes & Mkrtichian (2005) were able to confirm the presence of RV variations in only five individual spectral lines, two of which remained unidentified. The authors found the highest RV amplitude of 400 m s^{-1} in an unidentified line at λ5471.42 Å but could not detect pulsations in strong doubly ionized REE lines which show prominent variability in other roAp stars. In addition to its remarkably low-amplitude photometric pulsational variations, 10 Aql seems to exhibit an unusual spectroscopic pulsational behaviour, making this star perhaps an intermediate object between high-amplitude roAp stars and apparently constant non-pulsating magnetic Ap stars.

10 Aql was chosen as a target for an extensive observing campaign by the Canadian photometric space telescope MOST (Microvariability & Oscillations Stars) (Walker et al. 2003). The star was observed as a primary target in 2006 June–July, and nearly 120 000 10-s exposures were collected during 31 d at a sampling interval of 20 s. The frequency analysis by Huber et al. (2008) revealed three definite periodicities and two candidate frequencies (see Table 1). Huber et al. showed that the two largest amplitude peaks reported by Heller & Kramer (1990) are 1 d^{-1} aliases of the intrinsic stellar frequencies f_1 and f_2. The third significant MOST frequency, $f_3 = 1.43$ mHz, has not been detected in previous photometric observations of 10 Aql. The lack of rotational modulation signal in the MOST data confirms the suspected slow rotation of the star. Huber et al. (2008) derived an improved value of the large frequency separation, $\Delta \nu = 50.95$ µHz, and have compared the observed frequencies with the predictions of the theoretical models of non-adiabatic, magnetically distorted p-modes (Saio 2005).

With the aim to improve the frequency analysis, study line profile variations and perform a tomographic analysis of the pulsations in the atmosphere of 10 Aql, we have organized a ground-based spectroscopic observing campaign simultaneously with the MOST observations. Using high-resolution spectrographs at 4- and 8-m telescopes, we have collected a superb observational material with very high signal-to-noise ratio (S/N), wide wavelength coverage and a high spectral resolving power presented in Table 1. This combination of the data quality and time coverage has been never achieved before for any roAp star.

Preliminary results of our pulsation study of 10 Aql were reported by Sachkov et al. (2007). In that paper we outlined the frequency analysis procedure and discussed the main pulsation properties of 10 Aql, such as the presence of a node-like behaviour in the bisector variations, phases and amplitudes of RV variation for different

REE ions. Subsequently, Elkin, Kurtz & Mathys (2008) published an analysis of a short spectroscopic UVES time series of 10 Aql. These data, covering only 2 h, were analysed without taking the multiperiodic character into account. The pulsation frequency of 1.428 mHz adopted by Elkin et al. coincides with neither of the two highest amplitude pulsation modes in our data, but is close to the frequency f_3 identified by Huber et al. (2008) and by our spectroscopic analysis (see below).

The present paper is organized as follows. In Section 2 we describe spectroscopic observations and data reduction. Section 3 describes methodology of the line identification and RV measurements. The frequency analysis is outlined in Section 4. We establish a relation between photometric and spectroscopic variations of 10 Aql in Section 5. Line profile variations, indicating a pulsation node in the stellar atmosphere, and the discovery of a remarkable asymmetry in the Nd III lines are presented in Section 6. The paper ends with conclusions and discussion in Section 9.

2 OBSERVATIONS AND DATA REDUCTION

2.1 Time-series of UVES spectra

The main set of observational material analysed in this paper was obtained at the ESO 8-m VLT Unit Telescope 2 (UT2) using the UVES spectrograph. 10 Aql was observed for about 4 h during each of the following four nights in 2006: July 3, 9, 15 and 17. Each subset of observations consisted of 211 stellar exposures, followed by a ThAr lamp spectrum. We have used UVES in the 600-nm red-arm setting, that provided access to the 4980–6980 Å spectral window. The wavelength coverage is complete, except for a ≈100-Å gap centred at λ6000 Å. To facilitate the analysis of the narrow line profiles of 10 Aql and to improve the wavelength stability we used the UVES image slicer no. 3, resulting in a spectral resolving power of $\lambda/\Delta\lambda \approx 115\,000$.

10 Aql was observed with exposure times of 40 s. The fast readout mode of the UVES CCDs (625 kpixel s^{-1}, 4-port, low gain) reduces the overhead to about 29 s, resulting in a time resolution of 69 s. The typical S/N of individual spectra is 250–300 at $\lambda = 5000$–5500 Å.

Reduction of the UVES spectra utilized a set of echelle spectral processing routines developed by Tsymbal, Lyashko & Weiss (2003) and Lyashko, Tsymbal & Makaganuik (2007). Their code performs the standard reduction steps [averaging of calibration frames, determination of the echelle order position, bias subtraction, flat-fielding, extraction of one-dimensional (1D) spectra and wavelength calibration] and is optimized to treat the UVES slicer spectra. Further details of the application of this spectral reduction package to the time-resolved UVES observations of roAp stars are given by Ryabchikova et al. (2007b). This paper also details the final reduction step in which we improve continuum normalization of the individual time-resolved spectra obtained in the same night. Observations were obtained in different nights, hence we have carried out an additional continuum rectification correction to achieve a global consistency of the continua in all 844 UVES spectra.

Our data set of the UVES time-resolved spectra was complemented with the observations obtained in the context of program 077.D-0150 (Elkin et al. 2008) on July 24, which were taken with the instrumental set-up identical to ours and consist of 105 exposures obtained with the same exposure time and sampling as in our observations. These spectra along with the appropriate calibrations were retrieved from the ESO Archive and were subsequently processed in the same way as our own observations. Thus, a total of 949

high-quality UVES spectra are available for the pulsational analysis of 10 Aql.

2.2 Time series of SARG spectra

In addition to the UVES time series, 10 Aql was observed at high resolution with the spectrograph SARG at the 3.55-m Telescopio Nazionale Galileo (TNG) at the Observatorio del Roque de los Muchachos (La Palma, Spain) in the three consecutive nights of 2006 July 14–16. The total number of echelle spectra obtained with the SARG is 206. The star was monitored for 2.0–3.3 h using 70-s exposure times in each of the three nights. Including the 50-s overhead, the time resolution of these observations is 120 s. The SARG spectra cover the range of 4572–7922 Å without gaps with a resolving power of about 86 000. The typical S/N achieved for individual exposures is 90–150 at $\lambda = 5000$–5500 Å.

The spectra were reduced with standard procedures for spectroscopic observations which are part of the Image Reduction and Analysis Facility package of NAOA in the same way as in Leone & Catanzaro (2004). The post-processing of 1D extracted SARG spectra was performed consistently with the UVES spectra.

3 LINE IDENTIFICATION AND RADIAL VELOCITY MEASUREMENTS

To perform a careful line identification and to choose suitable lines for pulsation analyses, we have synthesized the whole spectral region with the model atmosphere parameters $T_{\rm eff} = 7550$ K, $\log g = 4.0$, and abundances from Ryabchikova et al. (2000). The mean magnetic field modulus of $\langle B \rangle = 1.5$ kG (Kochukhov et al. 2002) was adopted. Atomic data were extracted from the Vienna Atomic Line Database (VALD; Kupka et al. 1999), the revised atomic parameters for Nd III were taken from Ryabchikova et al. (2006) and the synthetic spectrum calculations were carried out with the SYNTHMAG code (Piskunov 1999; Kochukhov 2007b).

We have measured RVs using the centre-of-gravity technique as outlined by Kochukhov & Ryabchikova (2001a). A relatively low pulsation amplitude and a small number of spectral lines showing pulsation signatures seriously limited the usability of identification lists developed for other roAp stars. Therefore, we started by measuring practically all spectral lines (about 2000) in the July 3 time series in order to find lines with useful pulsation signatures. It turns out that the total number of such lines, both blended and unblended, is about 150. Most of the other lines belong to iron-peak elements which do not show significant RV variations or are blended to an unacceptable degree.

It is a well-known fact that spectroscopic pulsational variability of typical roAp stars is dominated by the lines of rare earth ions, especially those of singly and doubly ionized Pr and Nd, which are strong and numerous in the roAp spectra (see, for example, Savanov, Malanushenko & Ryabchikova 1999; Kochukhov & Ryabchikova 2001a). 10 Aql is different in this respect from other roAp stars. REE lines are weak, in particular those of the first ions. Their equivalent widths are confined between 2 and 12 mÅ. The Pr and Nd overabundance inferred from the lines of the first ions does not exceed 1.0 dex. RV measurements from these very weak lines often have insufficient precision for the purpose of our investigation. Therefore, we used for our further analyses only the lines with an equivalent width larger than 5 mÅ. The line identification list compiled for the July 3 spectra was then applied to all other UVES observations, using consistent central wavelengths and mea-

surement windows. For strong and intermediate-strong lines our measurements of individual RVs have an internal accuracy of up to 10 m s^{-1}.

We have unambiguously detected pulsations in the core of Hα and in the lines of Y II, La II, Ce II, Pr III, Nd II, Nd III, Sm II, Eu II, Gd II, Tb III and Dy III. All lines show strong changes in RV amplitude, indicative of beating between several excited modes. Typical observed semi-amplitudes, averaged over the whole duration of our spectroscopic monitoring, range from 50 to 150 m s^{-1}. During the periods of constructive interference amplitudes approach 400 m s^{-1} for some REE lines.

Remarkably large RV amplitudes – 350 m s^{-1} on average – were measured for the Dy III 5345, 5556, 5730 Å lines and for the two unidentified lines at λ5373.02 and 5471.40 Å. The identification of 5345 and 5556 Å lines is based on the unpublished data kindly provided by A. Ryabtsev (Institute of Spectroscopy RAS). All these lines have equivalent widths in the range of 9–12 mÅ and their depths are less than 9 per cent of the continuum. The pulsational characteristics of the two unidentified features are similar to those of Dy III and a few Ce II lines. Without any doubt both unidentified lines belong to the REE species. Both features are measured in HD 24712 (Ryabchikova et al. 2007a) and their pulsational characteristics are much closer to Dy III lines than to Ce II lines. In γ Equ, too, Dy III 5730 Å and 5373.02, 5471.40 Å lines have similar pulsational amplitudes and phases, which differ significantly from those of Ce II lines. Thus, we suggest that the unidentified lines at 5373.02 and 5471.40 Å belong to the Dy III spectrum.

The strong Nd III and Pr III lines in 10 Aql, that usually exhibit the largest amplitudes in roAp stars, have amplitudes below 100 m s^{-1} and probably form in the nodal area (see Section 6). The strongest Nd II lines in the observed spectral range have equivalent widths smaller than 7 mÅ, while Pr II lines are not measurable at all. Hence, the blending problem in this star becomes more serious. Even slight blending of a REE feature may significantly decrease the inferred amplitude (Kochukhov et al. 2002). Taking into account the observed pulsation amplitudes and accuracy of RV measurements (defined primarily by the spectral line strength and central wavelength), we have selected 65 lines for the frequency analysis and the study of the pulsational wave propagation through the stellar atmosphere. This line list is provided in Table 4.

We also report on the analysis of a subset of non-pulsating lines belonging to the iron-peak elements, Ca and Ba. These results, given in Table 5, demonstrate the overall accuracy of our pulsation measurements. Among the lines with definite RV variation the lowest amplitude of 15 ± 1 m s^{-1} is detected in the strong Y II 5662.9 Å line ($W_\lambda = 57$ mÅ). In comparison, for the non-pulsating lines of the same intensity the amplitudes are at the level of 2–4 m s^{-1}. We consider this to be the upper limit of pulsation amplitude for the lower atmosphere of 10 Aql. Note that although for many non-pulsating lines the free-period search yields values comparable to real frequencies of 10 Aql (see next section), the false alarm probability (FAP; Horne & Baliunas 1986) of such signals is always large (Prob, listed in the table is small).

In addition to the centre-of-gravity RV measurements, we studied bisector velocities across the Hα line core and profiles of the strongest REE spectral lines.

The UVES and SARG data sets overlap for about 1 h in the night of July 15. The RVs from the two spectrographs agree within the error bars, where the RV measurements with the SARG spectra are less accurate due to a lower S/N.

Table 2. Journal of spectroscopic observations of 10 Aql.

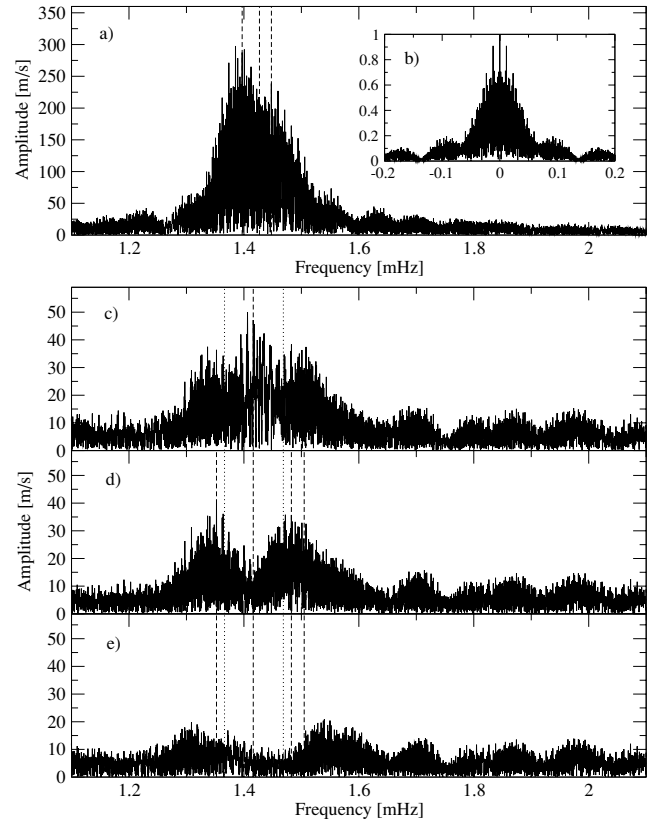| Date	Start HJD (245 0000+)	End HJD (245 0000+)	Spectral range (Å)	N spec.	Exposure time (s)	Time resolution (s)	Typical S/N	Instr.
2006 July 3	3919.60523	3919.77510	4980–6980	211	40	69	330	UVES
2006 July 9	3925.64884	3925.81471	4980–6980	211	40	69	260	UVES
2006 July 15	3931.62381	3931.79193	4980–6980	211	40	69	240	UVES
2006 July 17	3933.63894	3933.80793	4980–6980	211	40	69	300	UVES
2006 July 24	3940.64279	3940.72682	4980–6980	105	40	69	300	UVES
2006 July 14	3930.52693	3930.61096	4572–7922	59	70	120	150	SARG
2006 July 15	3931.52970	3931.66690	4572–7922	86	70	120	90	SARG
2006 July 16	3932.49220	3932.58039	4572–7922	61	70	120	140	SARG

Table 3. Secure (bold) and tentative (italics) spectroscopic pulsation frequencies of 10 Aql determined from the analysis of the average RVs of seven REE ions derived from the UVES spectra (second and third columns) and from the average RVs of five Dy III lines measured in the UVES+SARG spectra (fourth and fifth columns). The numbers in brackets give the error in units of the last significant digit.

Id	ν (mHz)	Ion	ν (mHz)	S/N
	UVES data		UVES+SARG data, Dy III	
f_1	**1.447 842(4)**	All	**1.447 87(1)**	39.8
f_2	**1.396 883(3)**	All	**1.396 84(1)**	48.2
f_3	**1.427 082(7)**	All	**1.427 11(1)**	21.2
f_4	*1.4 108*	Dy III, Tb III	*1.416 27(3)*	7.9
	1.4 341	Ce II		
	1.4 177	Sm II		
f_5	*1.3 127*	Dy III	*1.352 27(3)*	6.6
	1.3 367	Ce II		
	1.3 424	Sm II		
	1.3 600	Nd III		
f_6			*1.482 60(3)*	6.0
f_7	*1.5 048*	Dy III	*1.504 88(5)*	4.3
	1.5 125	Sm II		
	1.5 252	Gd II		

Figure 1. The amplitude spectra for the average Dy III RVs inferred from the UVES+SARG observations. (a) The DFT of the RV signal; (b) spectral window; (c) the residual amplitude spectrum obtained after pre-whitening the three main frequencies f_1–f_3 (dashed lines); (d) the residual amplitude spectrum obtained after pre-whitening the four frequencies f_1–f_4; (e) the residual noise after pre-whitening the seven frequencies f_1–f_7 from Table 3. These frequencies are indicated by dashed lines, while the dotted lines correspond to the MOST candidate frequencies.

4 FREQUENCY ANALYSIS

We carried out the frequency analysis by applying the standard combination of discrete Fourier transform (DFT) and least-squares fitting. For each of the studied REE ions we found a number of lines showing clear pulsation signatures. Aiming to improve the S/N of the RV data, we subtracted linear trends from the measurements of different lines of the same ions and averaged these data. The RVs derived from the average of five Dy III lines turned out to be especially useful for the frequency analysis. In all nights of our UVES observations, 10 Aql exhibited a large variation in the RV amplitude, which often changed from <100 to 500–700 m s^{-1} in the course of a few hours. This behaviour, illustrated in Fig. 2 for Dy III, is caused by beating of several frequencies.

The total time-span of the spectroscopic data set is about 25 h, but the spectra were obtained in a period of 21 d and, thus, are characterized by a very low duty cycle. Despite the clarity of the pulsational RV variations, severe aliasing inhibits a secure identification of the frequencies from the spectroscopic data alone. For example, the peak with a highest amplitude is often found at 1.3853 mHz, which is a per day alias of the photometric frequency f_2. Fig. 1 illustrates this problem for Dy III.

The original motivation for simultaneous MOST and spectroscopic observations was to take advantage of the accurate photometric frequency information in the analysis of spectroscopic data. Therefore, we have adopted the three main MOST frequencies as the initial guess in a non-linear least-squares fitting procedure. Then, we optimized the amplitudes, phases and periods of the three frequency components for each REE ion. For a number of REE ions (Ce II, Nd III, Sm II, Eu II, Gd II, Tb III, Dy III) we were able to determine all three frequencies with a S/N = 10–60.

Table 4. Summary of our spectroscopic pulsational analysis of individual spectral lines in 10 Aql. The columns give central wavelengths in Å, followed by the free search period P with the respective error estimate σ_P derived with a least-squares fit. The corresponding probability of a periodic signal (Prob.) is calculated according to Horne & Baliunas (1986). The next three groups of columns give pulsation amplitudes and phases φ with the respective errors, determined with a simultaneous fit of three fixed pulsation periods indicated in the column head. Phases are given as a fractional pulsation period. The starting point for frequency calculations is HJD = 244 53919.60523.

	Free period			Fixed periods												
λ	P	σ_P	Prob.	$P = 11.931$ min				$P = 11.511$ min				$P = 11.679$ min				W_λ
(Å)	(min)			A	σ_A	φ	σ_φ	A	σ_A	φ	σ_φ	A	σ_A	φ	σ_φ	(mÅ)
Hα core																
6562.799	11.42 103	0.00010	1.0000	52	2	0.611	0.007	49	2	0.287	0.007	37	2	0.826	0.010	
Y II																
5662.934	12.03 117	0.00015	1.0000	15	1	1.100	0.013	5	1	0.797	0.035	4	1	1.251	0.026	57.3
La II																
5290.814	11.41 958	0.00037	0.9996	18	12	0.645	0.111	61	12	1.174	0.033	23	13	0.715	0.092	4.0
5377.074	11.68 604	0.00032	1.0000	27	13	0.434	0.078	78	13	1.195	0.027	81	14	0.742	0.028	5.2
5805.773	11.51 219	0.00023	1.0000	1	5	0.946	0.132	44	5	1.313	0.018	29	5	0.838	0.029	8.9
Ce II																
5037.803	12.03 132	0.00013	1.0000	77	7	0.861	0.015	61	7	0.480	0.019	74	7	0.986	0.017	6.3
5044.018	12.03 110	0.00007	1.0000	129	5	0.856	0.006	109	5	0.502	0.008	90	5	0.998	0.010	7.1
5274.231	12.03 107	0.00005	1.0000	263	5	0.888	0.003	186	5	0.555	0.005	141	6	1.055	0.007	12.7
5330.548	12.03 110	0.00009	1.0000	116	5	0.885	0.008	92	5	0.514	0.010	76	6	1.073	0.013	6.6
5468.391	12.03 106	0.00009	1.0000	189	7	0.893	0.007	131	7	0.524	0.009	100	8	1.043	0.013	7.5
5512.047	12.03 094	0.00008	1.0000	121	4	0.857	0.005	87	4	0.501	0.008	61	4	1.021	0.011	10.0
5695.846	12.03 110	0.00020	1.0000	182	20	0.824	0.018	132	20	0.444	0.025	111	21	0.991	0.031	3.2
Pr III																
5299.988	12.03 111	0.00021	1.0000	25	3	1.318	0.020	16	3	0.923	0.031	4	3	1.500	0.128	38.5
6090.013	11.33 115	0.00033	0.9945	13	3	1.352	0.042	18	3	0.903	0.031	9	3	1.441	0.062	19.1
6160.248	11.42 069	0.00029	1.0000	25	3	1.290	0.022	24	3	0.812	0.023	6	3	1.469	0.087	19.8
6195.596	12.04 860	0.00044	0.9991	20	5	1.243	0.042	5	5	0.804	0.145	8	5	1.593	0.105	35.2
Nd II																
5130.593	11.89 818	0.00011	1.0000	67	6	0.898	0.014	71	6	0.527	0.014	59	6	1.012	0.018	6.3
5293.156	11.48 186	0.00019	1.0000	34	4	0.845	0.019	25	4	0.524	0.027	14	4	1.017	0.052	6.1
5319.821	11.89 797	0.00014	1.0000	85	8	0.865	0.016	88	8	0.497	0.016	62	9	1.006	0.024	5.7
Nd III																
5102.435	12.03 096	0.00010	1.0000	35	1	1.215	0.009	10	1	0.862	0.029	2	2	1.484	0.126	110.
5286.742	12.03 119	0.00014	1.0000	88	7	0.913	0.014	82	7	0.588	0.015	54	8	1.068	0.025	8.6
5294.091	11.93 130	0.00015	1.0000	23	2	1.197	0.014	9	2	0.826	0.037	5	2	1.353	0.061	114.
5633.560	12.03 131	0.00015	1.0000	126	9	0.952	0.012	82	9	0.625	0.018	70	9	1.105	0.022	11.5
5677.167	12.03 097	0.00016	1.0000	91	7	1.011	0.013	56	7	0.650	0.021	36	7	1.197	0.032	23.3
5802.534	12.03 121	0.00010	1.0000	92	4	0.983	0.007	67	4	0.632	0.010	43	4	1.128	0.016	26.2
5845.020	12.03 085	0.00014	1.0000	83	5	1.001	0.010	52	5	0.682	0.016	21	5	1.205	0.039	35.6
5851.531	12.03 104	0.00010	1.0000	93	4	0.965	0.007	60	3	0.645	0.010	37	4	1.175	0.017	31.5
6145.042	11.93 123	0.00026	1.0000	42	4	1.049	0.018	20	4	0.757	0.038	16	4	1.210	0.049	90.5
6327.260	12.03 120	0.00009	1.0000	54	1	1.001	0.005	36	1	0.676	0.008	19	1	1.175	0.015	54.8
6550.239	12.03 126	0.00011	1.0000	24	1	1.039	0.008	13	1	0.721	0.013	7	1	1.179	0.025	58.2
6690.765	11.42 080	0.00028	1.0000	105	17	0.985	0.026	118	16	0.608	0.023	44	17	1.157	0.061	9.6
Sm II																
5052.757	12.03 104	0.00007	1.0000	172	5	0.682	0.005	189	5	0.333	0.004	149	5	0.837	0.006	14.1
5069.441	11.80 060	0.00007	1.0000	151	6	0.683	0.007	156	6	0.329	0.007	132	7	0.844	0.009	15.1
5103.082	12.03 093	0.00007	1.0000	145	3	0.692	0.004	146	3	0.323	0.004	107	3	0.836	0.006	16.5
5116.686	12.03 100	0.00008	1.0000	184	8	0.670	0.007	193	8	0.326	0.007	141	8	0.836	0.010	9.4
5759.515	11.42 085	0.00012	1.0000	106	8	0.688	0.012	134	8	0.299	0.009	78	8	0.844	0.017	7.8
Eu II																
5818.739	11.79 987	0.00025	1.0000	71	12	0.608	0.027	64	11	0.176	0.030	31	12	0.786	0.063	5.4
6173.043	11.89 795	0.00025	1.0000	63	7	0.594	0.019	55	7	0.216	0.022	28	7	0.767	0.044	9.3
6303.408	12.03 093	0.00020	1.0000	81	7	0.579	0.015	37	7	0.179	0.034	27	8	0.759	0.046	7.3
6437.670	12.03 094	0.00016	1.0000	72	5	0.588	0.011	48	5	0.226	0.017	32	5	0.818	0.025	26.1
6645.070	12.03 091	0.00009	1.0000	108	3	0.624	0.006	70	3	0.254	0.009	52	3	0.834	0.012	34.5

Table 4 – *continued*

λ (Å)	P (min)	σ_P	Prob.	A	σ_A	φ	σ_φ	A	σ_A	φ	σ_φ	A	σ_A	φ	σ_φ	W_λ (mÅ)
	Free period			P = 11.931 min				Fixed periods P = 11.511 min				P = 11.679 min				
Gd II																
5092.246	11.78 693	0.00008	1.0000	100	6	0.807	0.010	101	6	0.422	0.010	98	6	0.920	0.011	12.2
5372.208	11.78 713	0.00021	1.0000	28	8	0.719	0.049	66	8	0.204	0.021	68	9	0.831	0.023	5.6
5419.876	11.51 224	0.00020	1.0000	12	6	0.567	0.083	67	6	0.194	0.016	54	7	0.775	0.021	5.4
5469.707	11.64 521	0.00026	1.0000	29	12	0.691	0.067	88	12	0.217	0.023	82	13	0.819	0.025	5.0
5500.432	11.78 666	0.00022	1.0000	57	14	0.750	0.040	99	14	0.205	0.023	87	15	0.809	0.028	4.4
5583.669	11.78 669	0.00028	1.0000	69	12	0.754	0.028	57	12	0.302	0.033	45	12	0.847	0.044	5.7
5721.971	11.69 107	0.00024	1.0000	22	11	0.859	0.082	99	11	0.172	0.018	79	11	0.780	0.024	4.7
5733.856	11.69 121	0.00021	1.0000	121	14	0.841	0.019	92	14	0.434	0.024	99	14	0.947	0.023	9.9
5815.839	11.69 088	0.00022	1.0000	17	6	0.786	0.061	60	6	0.189	0.018	46	6	0.764	0.024	8.8
5840.468	11.51 229	0.00028	1.0000	15	13	0.725	0.144	98	13	0.212	0.022	69	13	0.761	0.032	5.1
5856.964	11.42 080	0.00020	1.0000	13	8	0.815	0.096	84	8	0.169	0.016	59	8	0.714	0.023	6.4
5860.725	11.69 118	0.00024	1.0000	56	13	0.799	0.039	66	13	0.226	0.033	87	14	0.771	0.026	7.8
5877.231	11.78 691	0.00018	1.0000	34	7	0.723	0.035	70	7	0.219	0.017	70	7	0.800	0.018	6.3
5913.517	11.78 672	0.00020	1.0000	51	7	0.771	0.022	64	7	0.257	0.018	52	7	0.863	0.022	9.1
Tb III																
5505.370	12.03 100	0.00006	1.0000	238	6	1.339	0.004	156	6	1.024	0.007	117	6	1.510	0.009	15.0
5847.221	12.03 102	0.00013	1.0000	355	19	1.346	0.009	257	19	1.042	0.012	163	20	1.569	0.020	10.5
6092.884	11.80 040	0.00014	1.0000	115	7	1.344	0.010	114	7	0.990	0.010	75	7	1.508	0.015	10.5
6687.648	12.13 203	0.00046	0.8814	133	32	1.386	0.039	130	32	1.006	0.039	84	32	1.501	0.062	8.2
Dy III																
5345.374	12.03 102	0.00006	1.0000	228	5	0.850	0.004	217	6	0.513	0.004	164	6	1.008	0.006	8.9
5373.015	12.03 108	0.00006	1.0000	315	9	0.857	0.005	268	9	0.524	0.006	212	10	1.030	0.008	9.0
5471.416	12.03 106	0.00009	1.0000	341	13	0.888	0.006	286	13	0.523	0.008	196	14	1.024	0.012	9.0
5556.132	12.03 097	0.00008	1.0000	349	11	0.875	0.005	311	11	0.537	0.006	208	11	1.045	0.009	7.8
5730.335	12.03 104	0.00009	1.0000	319	8	0.889	0.004	273	8	0.540	0.005	200	9	1.051	0.007	12.0
Ho III																
5543.732	12.03 096	0.00010	1.0000	77	3	1.098	0.007	63	3	0.750	0.008	39	3	1.278	0.014	11.3

The formal accuracy of the periods determined for each of these ions is comparable or better than for the MOST photometry. We attribute this result to a much higher S/N achieved in the spectroscopic observations. In Table 3 we report the weighted mean of the spectroscopic pulsation frequencies in 10 Aql. A comparison with MOST (Table 1) shows that all our frequencies deviate by less than 1σ from the photometric results.

After pre-whitening the RV curves with the three main frequencies, all REEs show residual amplitude peaks in the 1.3–1.5 mHz range. In the UVES data the residual RV variations have amplitudes between 10 and 50 m s^{-1}, and show different frequencies at the S/N level of 3–4, depending on the ion. None of these frequencies coincides with the candidate MOST frequencies f_i and f_j. Accurate determination of the low-amplitude frequencies in spectroscopy is hampered by the aliasing problem. Nevertheless, we note that the most promising spectroscopic candidate frequency is $f = 1.3367$ mHz. Variation with this period (or its aliases) is seen in Dy III, Ce II, Sm II and Nd III. This frequency coincides with a sidelobe of a MOST orbital frequency harmonics and therefore does not contradict the space photometry reported by Huber et al. (2008), because these frequency ranges were excluded deliberately from the analysis. The other candidate spectroscopic frequencies are 1.411–1.434 mHz (seen in Dy III, Tb III, Ce II and Sm II) and 1.505–1.525 mHz (Dy III, Sm II and Gd II). They are not observed in the MOST data. The amplitudes and phases of the three main periods do not change beyond their formal error bars when additional low-amplitude frequencies are included in the fit.

A lower S/N and the specific temporal coverage of the SARG observations close to minimum RV due to beating effects do not allow us to use these RV measurements for all REE ions. However, we found that the highest amplitude Dy III lines allow to analyse the complete set of UVES+SARG data and improve the frequency solution.

Three practically unblended Dy III lines (5345.37, 5556.13 and 5730.34 Å) as well as two unidentified lines (5373.02 and 5471.42 Å) that we propose to identify also as Dy III were chosen for RV measurements. The linear instrumental trends were subtracted for each night of observations. Because of the negligible phase shift between the RV curves of these lines we can average the RV's and weight data according to the individual errors to increase the accuracy of the frequency analysis. After subtracting the three main frequencies, that are the same as detected by MOST or by using only the UVES data, the residual RV variations show amplitudes clearly exceeding the noise level in three distinct regions, indicating the presence of additional signal in the data (see Fig. 1c). To reduce the aliasing problem the program SIGSPEC (Reegan 2007) was applied to the residuals for an accurate determination of additional low-amplitude frequencies. The main functionality of SIGSPEC is the evaluation of the probability that a signal in the Fourier domain is not caused by random noise by taking frequency, amplitude and phase information into account, yielding a quantity called spectral significance. In addition, SIGSPEC employs an anti-aliasing correction procedure, in which several trial frequencies (starting with the one showing the highest significance) are pre-whitened. The most
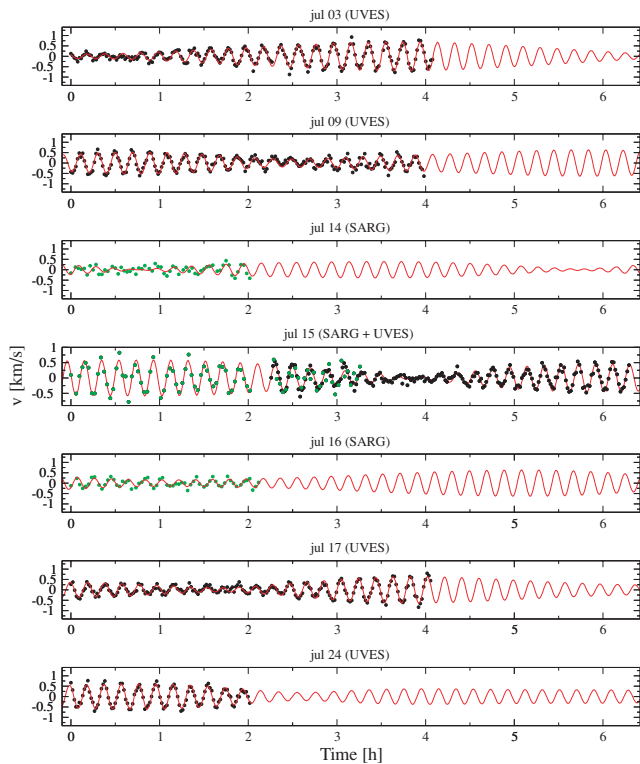
Figure 2. The average RV variation of Dy III lines during seven nights of spectroscopic observations. The measurements are shown with black (UVES) and green (SARG) dots. The solid curve represents a least-squares fit of seven pulsation frequencies detected in 10 Aql.

probable frequency is assumed to be that which results in the lowest residual scatter of the data after pre-whitening. The program PERIOD04 (Lenz & Breger 2004) was used to check the SIGSPEC solution by calculating a multisine fit, allowing simultaneously to improve frequency, amplitude and phase of all detected signals.

For the residual RV variations, the selection of the frequency at $f = 1.4163$ mHz yields the lowest residual scatter. Note that this peak does not coincide with the highest peak in the amplitude spectrum (see Fig. 1c). Choosing another (e.g. the highest amplitude) frequency in this pre-whitening step will yield an almost completely different set of subsequent frequency values, but not reaching the same low noise level.

After pre-whitening of this signal two additional power excess regions remain (Fig. 1d). In total, three additional frequencies are needed to obtain residuals that show only noise (Fig. 1e). Tables 3 and 4 list all derived frequencies.

Fig. 2 shows a direct comparison of the RV observations and a seven-frequency solution, while Fig. 3 displays an amplified part of the observations near beating. Clearly, using only the three definite MOST frequencies is not sufficient to fully reconstruct the observed variations. While the seven-frequency fit is an improvement one has to stress that the frequency identification is insecure due to the severe aliasing effects and it strongly depends – as was already mentioned – on the pre-whitening sequence.

The discrepancy that none of the spectroscopically identified low-amplitude frequencies shows up in the MOST photometry can be explained by their expected amplitude in the photometry of about 30 ppm, which is about three times the noise level as stated by Huber et al. (2008). This estimate comes from scaling the RV am-

plitude of f_1 to the highest peak in the residual RV variations and assuming the amplitude ratios to be similar in photometry and spectroscopy. Therefore, this additional signal might be lost in the noise. On the other hand, it has also been suggested that spectroscopic and photometric observations, probing different layers of the stellar atmosphere, can yield different pulsation frequencies (Kurtz, Elkin & Mathys 2006). The clear lack of signal around 1.41 mHz in photometry, but which shows a convincingly high S/N in spectroscopy, could support this concept. That neither of the photometric candidate frequencies f_i nor f_j contribute to a good frequency solution for the RV variations corroborate that these frequencies are insecure, as was stated by Huber et al. (2008), or indicate that the amplitude scaling between photometry and spectroscopy is not as simple as we assumed. The spectroscopic data does not show any signal close to the third frequency ($\sim$1.24 mHz) proposed by Heller & Kramer (1990) and Belmonte et al. (1991). This is consistent with the results obtained by MOST.

As already noted, our dominant pulsation frequencies are consistent with those determined from the analysis of the MOST data, but we find systematically different amplitude ratios. The MOST results indicate that f_1 shows the highest amplitude and f_2 is the second highest: $A_1/A_2 = 1.1 \pm 0.1$ (Huber et al. 2008). However, in spectroscopy $f_2(P = 11.931$ min) exhibits the highest amplitude for nearly all lines ($A_1/A_2 = 0.7$–0.9). One can speculate that this discrepancy comes from a different sampling of the propagation regions in spectroscopy and photometry, respectively.

After improving the estimate for the three high-amplitude pulsation frequencies in 10 Aql, we determined amplitudes and phases (expressed as fractional pulsation period) for 65 selected lines based on this solution and using $\cos\{2\pi[(t - t_0)/P - \varphi]\}$ to fit the RV curves instead of the usual $\cos\{2\pi[(t - t_0)/P + \varphi]\}$, which correlates a larger phase to a later RV maximum. The reference time adopted for pulsation phase calculations is HJD $= 244\,53919.60523$. The results of the frequency analysis of individual lines in the data set containing all five UVES nights are reported in Table 4. For all measured lines we also performed a period search with the periodogram method, which allowed us to estimate the probability of the pulsation signal detection (1 – FAP; see Horne & Baliunas 1986). With a few exceptions, the FAP is below 10^{-4}.

Table 4 also gives the equivalent width of the pulsating lines. Notably, all REE lines with amplitudes significantly exceeding 100 m s^{-1} are very weak (equivalent width $\sim$10 mÅ or less). Their analysis becomes possible thanks to a high S/N achieved in the time-resolved UVES spectra of 10 Aql.

5 PHASE RELATIONS BETWEEN PHOTOMETRY AND SPECTROSCOPY

Our spectroscopic time series were carried out simultaneously with the MOST photometry. This gives us a unique possibility to derive directly the phase lag between the photometric and spectroscopic pulsational variations, which provide useful constraints for subsequent modelling of oscillations. Earlier attempts of similar simultaneous analysis of the spectroscopic and photometric observations were carried out only for one roAp star – HD 24712 – by Matthews et al. (1988) using ground-based photometry and by Ryabchikova et al. (2007a) using MOST photometry.

The high S/N and spectral resolution of the present observations of 10 Aql allow us to derive phase lags for individual spectral lines, sampling different atmospheric layers. In order to minimize the influence of the higher (with respect to the spectroscopic

observations) point-to-point scatter of the photometric observations, we have constructed an artificial light curve based on the frequencies, amplitudes and phases of the three dominant pulsation modes (f_1, f_2 and f_3) as derived by a multisine fit to the MOST data. In a next step the artificial time series were cross-correlated with the RV observations of the individual spectral lines. The time interval for the cross-correlation was chosen from plus to minus 11.93 min (the period of the main photometric frequency, f_1), with an increment of 1 s. We note that the significant modulation of the pulsation amplitude due to beating of several frequencies helps to distinguish between a phase lag of e.g. -0.2 and $+0.8$, which is impossible for a monoperiodic star.

The results of the cross-correlation analysis for the representative set of spectral lines are given in Table 6, where we define the phase lag as the difference between the RV maximum of a given line and the photometric maximum, expressed in seconds or as a fractional main pulsation period $P = 11.93$ min. The error of

Table 5. Summary of the frequency analysis of non-pulsating lines in 10 Aql. The columns give central wavelengths in Å, followed by the free search period P with the respective error estimate σ_P derived with a least-squares fit. The corresponding probability of the periodic signal (Prob.) is calculated according to Horne & Baliunas (1986). The last three columns give an estimate of the RV amplitude and error, and equivalent width of the line.

λ (Å)	P (min)	σ_P	Prob.	A (m s^{-1})	σ_A	W_λ (mÅ)
Ca I						
6162.176	11.53066	0.00061	0.0015	6	2	127
Ca II						
5019.981	14.34773	0.00075	0.0000	4	1	112
5021.147	14.27341	0.00072	0.1659	7	2	47
Ti I						
5036.454	13.59938	0.00068	0.6997	12	3	10
5038.397	14.34091	0.00081	0.5762	10	3	9
Ti II						
5336.793	11.57725	0.00052	0.1716	5	2	55
5418.776	12.31386	0.00072	0.0036	6	2	35
Cr I						
5296.691	11.72380	0.00049	0.0079	5	1	59
5297.371	12.97623	0.00097	0.0000	3	1	93
5300.744	14.27558	0.00084	0.5068	5	2	33
5312.854	11.56547	0.00042	0.1617	8	2	26
5318.385	11.78757	0.00037	0.6640	7	1	36
5348.325	11.84174	0.00053	0.0000	6	2	67
Cr II						
5305.869	11.95541	0.00056	0.0013	4	1	71
5310.692	11.69145	0.00050	0.0019	5	1	55
5313.583	11.68307	0.00065	0.0000	3	1	75
Fe I						
5410.912	12.19297	0.00068	0.0001	5	1	84
5415.204	12.08059	0.00064	0.0102	4	1	111
Fe II						
5414.075	12.11682	0.00058	0.0007	5	1	42
Co I						
5331.452	11.57328	0.00061	0.0238	12	4	14
5342.701	11.88451	0.00058	0.0000	5	2	30
5347.496	11.59717	0.00059	0.0165	9	3	12
Ni I						
5035.359	11.95589	0.00046	0.2132	7	2	21
Ba II						
5853.684	11.85784	0.00064	0.0000	16	5	32

the phase lag determination was estimated as follows. We added a normally distributed random signal to both the spectroscopic and photometric data assuming that the noise amplitude corresponds to the observational error. For spectroscopy the error was derived from the RV determinations, and for photometry the MOST team recommended to use 2 per cent of the signal. A phase lag was derived from these noisy data and repeated 200 times. The resulting standard deviation was adopted as an error of the phase lag determination.

In contrast to HD 24712, where the RV maxima for all lines preceded the photometric maximum, in 10 Aql the maximum of brightness occurs prior to the RV maxima but the phase lag itself depends strongly on the line considered. It is minimal ($\approx$40 s) for the Eu II 6645 Å line and gradually increases for other lines, reaching a maximum of 550 s in Tb III. The growth of the phase lag from Eu to Tb lines has the same character as in HD 24712. It probably traces the outward propagation of the pulsation wave through the atmospheric layers.

6 PULSATIONS IN SPECTRAL LINES

6.1 Phase–amplitude diagrams

The presence of chemical stratification in the atmospheres of Ap stars offers a unique possibility to resolve the vertical structure of pulsation modes. However, the line-forming regions for REE are difficult to derive. Atmospheric modelling for such purposes should account for chemical stratification, deviations from local thermodynamical equilibrium (LTE), magnetic field and, eventually, pulsation effects on the shape and intensity of spectral lines with substantial RV variability. The formidable difficulties of such an elaborated theoretical approach explain why up to now Nd and Pr line formation calculations accounting for non-LTE (NLTE) and magnetic field effects in chemically stratified atmosphere have been carried out only for two roAp stars, γ Equ and HD 24712 (Mashonkina, Ryabchikova & Ryabtsev 2005; Ryabchikova et al. 2007c).

The assumption that the line intensity or equivalent width represents a proxy of the relative formation heights, frequently used in early roAp pulsation studies (e.g. Kanaan & Hatzes 1998), is only justified for the same element, respectively ion. It is now well established that stratification effects are dominant in the atmospheres of cool Ap stars and, therefore, the formation region of the weak lines of one element is not necessarily located deeper in the atmosphere than for strong lines of another element. Consequently, discussing pulsation amplitude or phase versus line depth in context of pulsation modes can be grossly misleading.

Ryabchikova et al. (2007b) suggested a different approach to the pulsation tomography problem based on the assumption of a continuous amplitude versus phase relation for an outward propagating magnetoacoustic wave. They proposed to use phase–amplitude diagrams to diagnose the structure of pulsation modes based on the following arguments: if one neglects surface chemical inhomogeneity (which is a reasonable assumption for slow-rotating roAp stars), then both phase and amplitude may provide information on the relative line formation depth. For instance, a phase-independent growth of the amplitudes measured for groups of lines belonging to different chemical species corresponds to a standing wave in the layers where these chemical species are formed. In the case of a phase-dependent amplitude trend, the lines showing later RV maximum should originate higher in the atmosphere. In the general case the vertical pulsation structure of roAp stars is likely to be a superposition of standing and running waves, corresponding to the
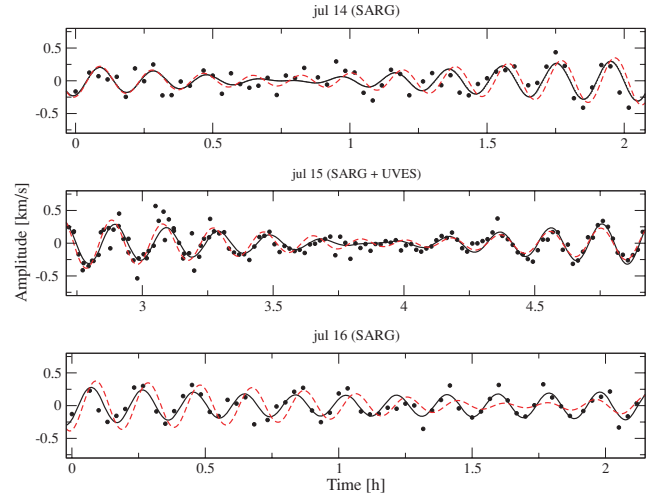
Table 6. Phase lags (in seconds and as a fractional main period $P = 11.93$ min) between the maxima of luminosity and RV variations of different chemical species in the atmosphere of 10 Aql.

Line	λ (Å)	Phase lag	
		Seconds	Fractional period
Eu II	6645	40 ± 8	0.05 ± 0.01
H I	6563	58 ± 12	0.06 ± 0.02
Sm II	5053	84 ± 24	0.12 ± 0.03
Gd II	5092	127 ± 45	0.22 ± 0.06
Dy III	5471	222 ± 9	0.29 ± 0.01
Dy III	5556	236 ± 18	0.31 ± 0.03
Ce II	5274	212 ± 14	0.32 ± 0.02
Dy III	5730	217 ± 17	0.32 ± 0.02
Nd III	5851	260 ± 25	0.40 ± 0.03
Nd III	5802	273 ± 23	0.40 ± 0.03
Nd III	5845	312 ± 17	0.44 ± 0.02
Nd III	5294	442 ± 30	0.59 ± 0.04
Nd III	5102	444 ± 43	0.62 ± 0.06
Pr III	5300	449 ± 18	0.70 ± 0.03
Tb III	5505	559 ± 7	0.77 ± 0.01

Figure 3. Part of the average Dy III RV curve (dots) around the amplitude minimum. The three-frequency and seven-frequency solutions are shown by dashed and solid lines, respectively.

decoupled magnetic and acoustic pulsation components which have different depth dependence (Sousa & Cunha 2008b). In the same star pulsations in certain ions may trace the standing, magnetic part of the wave while other ions may show predominantly the running, acoustic component. The phase–amplitude diagram method is well suited to characterize this behaviour thus offering the possibility of tracing the vertical properties of pulsation waves and studying the physics of magnetoacoustic oscillations from trends of pulsation velocity amplitude and pulsation phase without tedious assignment of the physical depth to each pulsation measurement.

The key assumption used in interpreting the phase–amplitude diagrams is that a later RV maximum corresponds to a higher line formation. This is supported by the gradual increase of pulsation phase with height from Hβ-, Hα cores to Nd II–III–Pr II–III lines (e.g. Sachkov et al. 2006) in practically all roAp stars where formation heights of pulsating lines could be constrained independently of the pulsation analysis (Mashonkina et al. 2005; Ryabchikova et al. 2007c). Since the chemical properties of most roAp stars are quite similar (Ryabchikova et al. 2004) and their phase–amplitude dependences are also comparable (Ryabchikova et al. 2007b), the assumption of continuous outward increase of pulsation phase appears to be reasonable from the empirical point of view. On the other hand, the general validity of this picture has been questioned in the theoretical work by Sousa & Cunha (2008a). These authors demonstrated that using a certain combination of the model parameters (not applicable to 10 Aql or to any other roAp star), one can obtain a complex superposition of standing and outwardly propagating waves which would mimic an inwardly running wave. This situation may complicate interpretation of the phase–amplitude diagrams, and the case of 33 Lib (Section 9.3) possibly represents an example of such complex situation. However, a more realistic theoretical modelling using pulsation and atmospheric parameters relevant for specific roAp stars is required to confirm the reality of such complex depth dependence of pulsation phase.

Similar to the analysis of 10 roAp stars presented by Ryabchikova et al. (2007b), we applied the amplitude–phase diagram method to 10 Aql. Furthermore, the availability of our rich spectroscopic observational material allows us to improve the precision of our previous analysis which was presented at the CP#Ap Workshop in 2007 by Sachkov et al. (2007), and for the first time to recover the amplitude–phase diagrams for several pulsation modes in the same roAp star. These diagrams are shown in Fig. 4 for the three main frequencies observed in 10 Aql.

For the purpose of comparison, we plot bisector measurements across the Hα core in the amplitude–phase diagrams constructed via centre-of-gravity measurements. These measurements provide us with a physical depth scale in the atmosphere because hydrogen is distributed homogeneously with height. The core of the Hα line is formed in the region between $\log \tau_{5000} \sim -2$ and $\log \tau_{5000} \sim -4.7$ according to NLTE calculations using the codes described in Mashonkina et al. (2007).

As in other roAp stars, measurable pulsation amplitudes appear in the layers where Eu II, La II and the core of Hα are formed, reach maximum and then show decrease of the amplitude. The phase increases by 0.2 across the Hα-line core while the RV amplitude grows by four–five times. We observe a running wave-like behaviour in this part of the stellar atmosphere. Above the formation height of the deepest point of the Hα profile ($r = 0.15$) the amplitude continues to grow rapidly without significant phase change. However, while in most other roAp stars the maximum RV amplitudes are observed in singly and doubly ionized Nd and Pr lines, in 10 Aql the maximum are seen for the lines of Ce II, Dy III and a couple of unidentified lines too, attributed by us to Dy III.

The lines of Nd and Pr are formed above the Dy III lines and show a RV amplitude rapidly falling to very small values. In even higher layers, the pulsation amplitude starts to grow again and reaches a new maximum in lines of Tb III. Simultaneously, the pulsation phase changes by ∼0.5 between the two maxima. This is a typical picture of a pulsation node in the stellar atmosphere: the phase changes by 180° while on both sides of the phase jump we observe comparable RV amplitudes. The presence of the node is supported by the bisector measurements in Nd III lines (see below). If the optical depth scale indicated by the core of the Hα line is valid for other lines too, then we expect that the pulsation node is located near or above the optical depth of $\log \tau_{5000} \sim -4.5$. However, it should be stressed that the amplitude and phase distributions with height in the atmospheres of roAp stars are expected to depend on
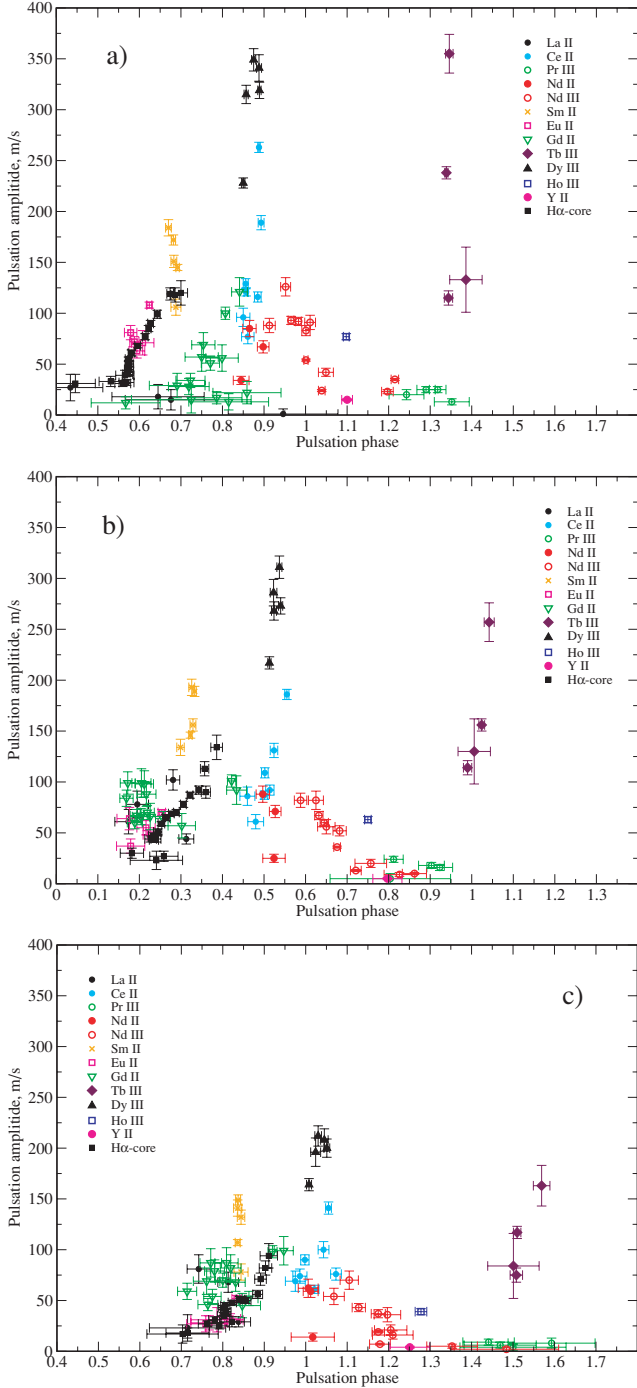
Figure 4. Amplitude–phase diagrams for three main pulsation periods in 10 Aql: $P = 11.93$ min (a), $P = 11.51$ min (b) and $P = 11.68$ min (c).

the local magnetic field strength and inclination (Sousa & Cunha 2008b). Thus, the inferred location of the node observed in the disc-integrated quantities represents the average of the local vertical pulsation structure which, possibly, exhibits substantial variation over the stellar surface. Ideally one should take this variation into account when determining the exact vertical location of the node.

Among the lines of elements other than rare earths only the strongest line of Y II, λ5662.9 Å, shows low-amplitude but definite pulsation. As in most other roAp stars (Ryabchikova et al. 2007b), this line overlaps with Pr III lines in the amplitude–phase diagrams.

The amplitude–phase diagrams for the three pulsation modes are very similar except, perhaps, Gd II and La II lines. Only four out of 14 Gd II lines have equivalent widths larger than 7 mÅ. Furthermore, most of Gd II lines are shallow due to substantial magnetic splitting; their central depth does not exceed 4–5 per cent. This makes pulsation measurements difficult. Pulsations can be detected in all Gd II, and it seems that this element shows higher amplitudes for the 11.51 and 11.68 min periods. The same situation is found for La II lines, which have even lower equivalent widths and lower RV amplitudes. This discrepant variation of the Gd II and La II lines for different frequencies may indicate a difference in the vertical extension of the corresponding modes. In particular, on the basis of these measurements, one may suspect that the frequency $f_2(P = 11.93$ min) corresponds to a pulsation mode located in higher atmospheric layers compared to f_1 and f_3. This agrees with the difference between photometric and spectroscopic amplitude ratios for f_1 and f_2.

6.2 Bisector variation

The RV amplitudes and phases across the Hα core are shown in Fig. 5 as a function of the normalized flux (scale at the bottom) and optical depth (scale at the top) for all three principal pulsation periods seen in 10 Aql. We find very similar behaviour for the three modes. In fact, the amplitudes of f_1 and f_2 are identical within error bars, whereas the amplitude of f_3 is slightly lower. This suggests that the three modes sample the hydrogen line core formation region in a similar manner.

Because of the weakness of most spectral lines, the only metal line suitable for a precise bisector analysis is Nd III 5102.43 Å. This line is deep enough and its wings are free from blends. In many roAp stars this Nd III line is blended with Nd II 5102.39 Å and should be used with caution. However, due to the overall weakness of the Nd II spectrum in 10 Aql, the blending effect is negligible.

Bisector measurements across the Nd III 5102 Å line profile are shown in Fig. 6. A phase jump of approximately 0.4–0.5 seems to be located in similar atmospheric layers for all three main frequencies. A bisector analysis provides an independent evidence for the pulsation node in the upper atmosphere of 10 Aql. This is the second case after 33 Lib (Mkrtichian, Hatzes & Kanaan 2003; Kurtz, Elkin & Mathys 2005; Ryabchikova et al. 2007b) of a pulsation node found in a roAp star located within the REE-rich cloud.

Nd III 5102 Å line provides the most clear signatures of the pulsation node: phase jump of ∼0.5 of the period accompanied by the minimum in RV distribution. The start of the phase jump is seen in other Nd III lines as illustrated by fig. 6 of Elkin et al. (2008). In Nd III 6145 Å line it also reaches ∼ 180°, however, we did not analyse this line due to its known blend with Si I line that influences bisector RV values. Another strong Nd III 6237 Å line was omitted from the bisector analysis, too, because it is blended in the red wing by one of Sm II, an element which also shows pulsation, but probably is formed deeper in the atmosphere (see Fig. 4).

In comparison to the bisector variation in the Hα core, the Nd III 5102 Å bisectors behave differently for the three modes. The amplitude in the outer wings is the highest for f_2, whereas the steepest phase jump is seen for f_3. Based on the location of the maximum change of the bisector phase further outside in the wings, we tentatively conclude that the node region is located somewhat deeper for the f_3 mode than for the other two frequencies.
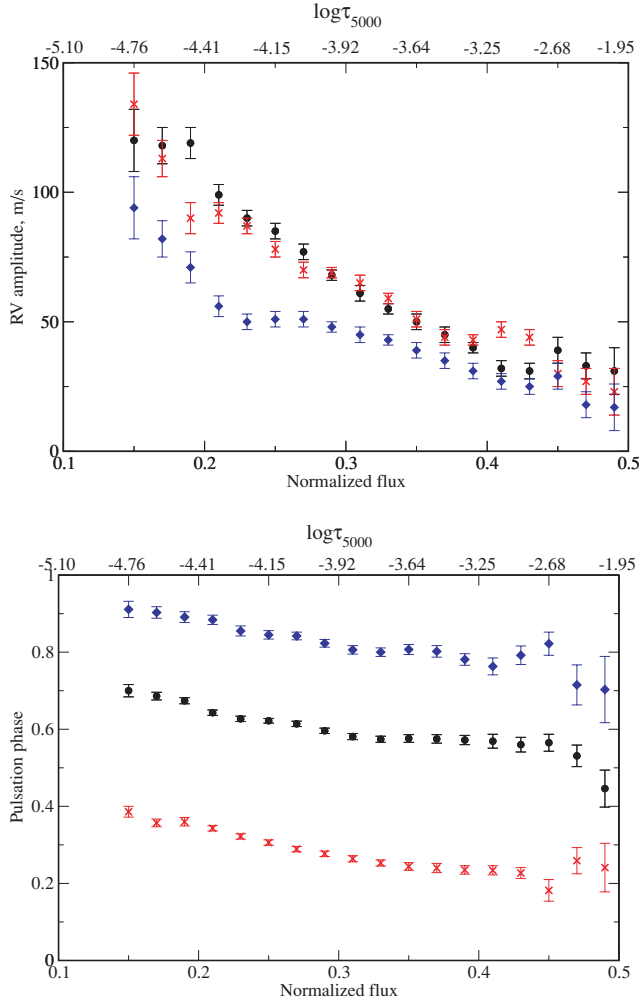
Figure 5. Bisector RV amplitudes (top) and phases (bottom) across the Hα core for the three main pulsation periods in 10 Aql: $P_1 = 11.51$ min (crosses), $P_2 = 11.93$ min (filled circles) and $P_3 = 11.68$ min (diamonds). The upper x-axis indicates the optical depth scale.
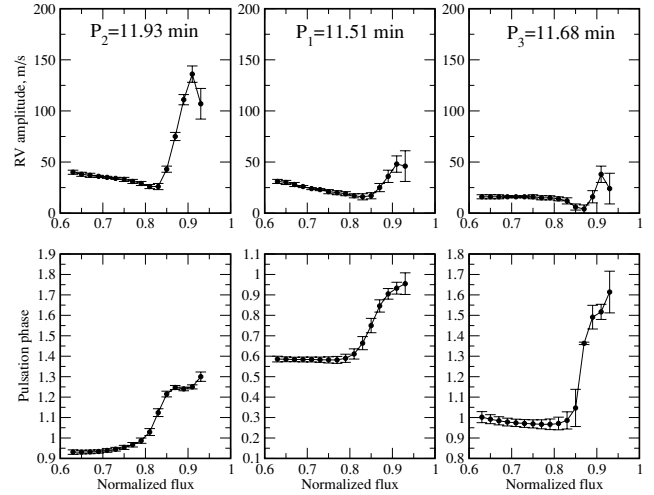

Figure 6. The RV amplitudes (top) and phases (bottom, expressed in as a fractional pulsation period) for Nd III 5102 Å.

7 ND III LINE PROFILE ASYMMETRY

Many cool Ap stars exhibit an unusually large broadening of the doubly ionized Nd and Pr lines, for which macroturbulent velocities of the order of $10 \, \mathrm{km \, s^{-1}}$ are often needed to achieve a good fit to the observed line profiles (Kochukhov & Ryabchikova 2001a; Ryabchikova et al. 2007b). The nature of this phenomenon is poorly understood, but it could be related to a turbulent instability in the upper atmospheric layers, possibly caused by the anomalous temperature gradient produced by a stratified distribution of the chemical elements. Although roAp stars are the ones most frequently showing this anomaly, it does not correlate with pulsation amplitude and is equally strong in stars in which pulsations at the level of 20–$30 \, \mathrm{m \, s^{-1}}$ are barely detectable (Kochukhov et al. 2008). As discussed by Kochukhov et al. (2007) the modulation of turbulence by the periodic contraction and expansion of the pulsating atmosphere in roAp stars with higher amplitudes explains the characteristic asymmetric line profile variation of the REE lines, first detected by Kochukhov & Ryabchikova (2001a) in γ Equ.

10 Aql, too, shows remarkably broad lines of Nd III, but curiously we find that the strongest of these lines are also extremely asymmetric. This effect is illustrated in Fig. 7 for several Nd III lines. In this figure we show rare earth line profiles in the spectra of four slowly rotating roAp stars: two stars with a small magnetic field, 10 Aql ($T_{\mathrm{eff}} = 7550 \, \mathrm{K}$, $\log g = 4.0$, $v_e \sin i = 2.0 \, \mathrm{km \, s^{-1}}$, $\langle B \rangle = 1.5 \, \mathrm{kG}$) and HD 12932 ($T_{\mathrm{eff}} = 7620 \, \mathrm{K}$, $\log g = 4.2$, $v_e \sin i = 2.0 \, \mathrm{km \, s^{-1}}$, $\langle B \rangle = 1.7 \, \mathrm{kG}$), and two stars with a large magnetic field, 33 Lib ($T_{\mathrm{eff}} = 7550 \, \mathrm{K}$, $\log g = 4.3$, $v_e \sin i \leq 2.0 \, \mathrm{km \, s^{-1}}$, $\langle B \rangle = 5 \, \mathrm{kG}$) and γ Equ ($T_{\mathrm{eff}} = 7700 \, \mathrm{K}$, $\log g = 4.2$, $v_e \sin i \leq 1.0 \, \mathrm{km \, s^{-1}}$, $\langle B \rangle = 4.1 \, \mathrm{kG}$) (Ryabchikova et al. 2007b). For a comparison the profile of the magnetically insensitive non-pulsating (or weakly pulsating) Fe I 5434 line is also shown for all stars. The wavelength scale is expressed in velocity units relative to the line centres. The strongest Nd III lines in 10 Aql at λ5102 and 5294 Å have a remarkable blue asymmetric wing reaching out to $-50 \, \mathrm{km \, s^{-1}}$. The red wing stops at $\approx 20 \, \mathrm{km \, s^{-1}}$ as do both wings in the Nd III lines in the other roAp stars shown in Fig. 7. In 10 Aql the blue wing asymmetry is still prominent in Nd III 6145 Å and gradually disappears for weaker Nd III lines. The profiles of strongly and weakly pulsating lines in HD 12932 and γ Equ are symmetric. In 33 Lib the weakly pulsating Fe I 5434 Å line is symmetric while REE lines have a small red asymmetry. In 10 Aql the non-pulsating Fe I 5434 Å line has a clearly asymmetric red wing.

The available information is insufficient to attribute REE line asymmetries either to non-radial pulsations or to an anisotropic turbulent velocity field. The sign of the asymmetry suggests an outward flow of Nd-rich material in the layers probed by the wings of strong Nd III lines. However, this effect can be mimicked by a non-isotropic velocity distribution of an ion stably stratified in the upper stellar atmosphere, as discussed by Michaud (1978) for Sr in hotter CP stars. A similar investigation is needed for REE in cool Ap stars to shed light on the abnormal shapes of strong Nd lines in 10 Aql.

8 ROTATIONAL MODULATION

A comparison of the average spectra obtained in five UVES nights over a period of about one month did not show any hint of line profile or RV changes on time-scales of days. This supports the study by Ryabchikova et al. (2005) who have used own mean longitudinal field measurements and data taken from the literature to argue for a long rotational period of 10 Aql. To search for long-term variations
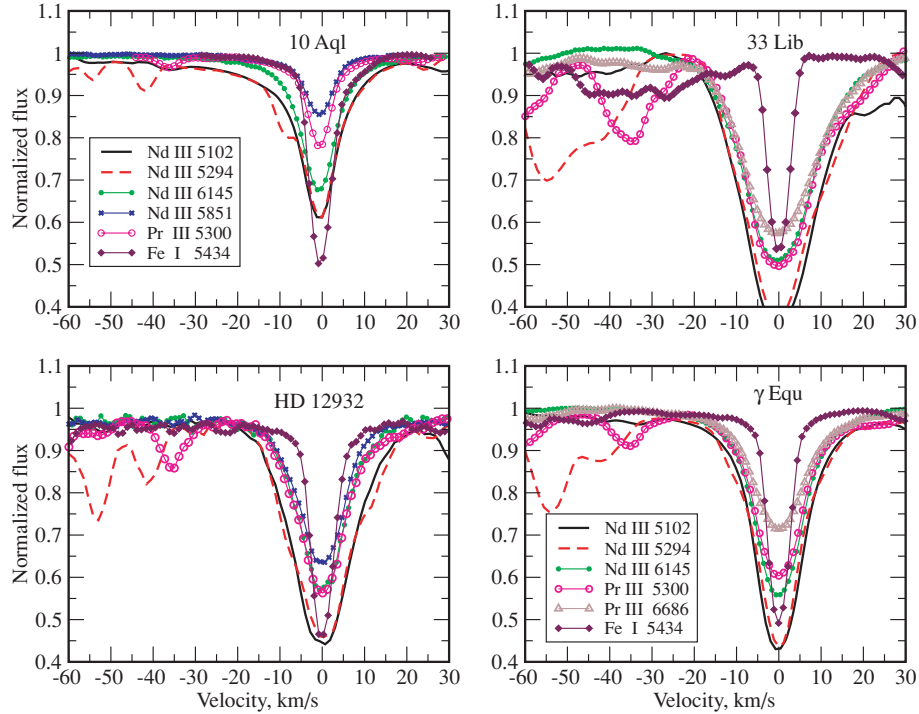
Figure 7. REE and Fe I line profiles in the spectra of the weakly magnetic roAp stars 10 Aql and HD 12923, and of stronger magnetic roAp stars 33 Lib and γ Equ.
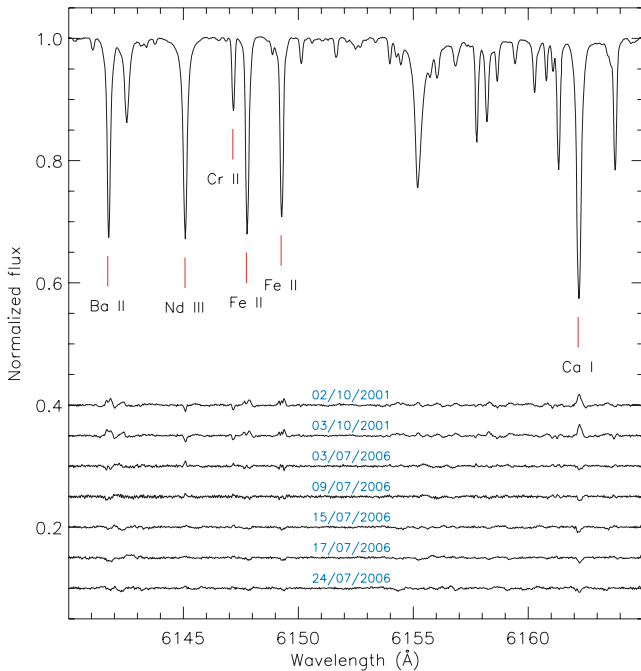

Figure 8. Comparison between the 10 Aql spectra obtained in 2001 and 2006. The upper plot shows the average spectrum, the residual spectra are plotted below. They are shifted vertically for a better visibility.

we have compared the average UVES spectra with observations obtained in 2001 with the Gecko coudé spectrograph at the 3.6-m Canada–France–Hawaii Telescope (Kochukhov et al. 2002). We introduced additional broadening to the latter spectra to compensate for the difference in spectral resolution between Gecko and UVES.

The global average spectrum of 10 Aql in the 6140–6165 Å region and the residual spectra to this average are presented in Fig. 8.

A signature of weak variability can be seen in the centres of few strong lines of Ca I, Fe II, Ba II, Nd III, as well as in the moderately weak Cr II line. We are confident that this variability is not an artefact due to using different spectrographs, because the intensity variations of Ca I, Fe II, Ba II lines are in *antiphase* with the variations of Nd III and Cr II lines. Possibly, this is another evidence for a rotational modulation in the spectra of 10 Aql, indicating a long rotation period.

9 DISCUSSION

9.1 Re-assessment of asteroseismic models

The additional spectroscopic frequencies could offer a new view on the large frequency separation $\Delta \nu$, a crucial factor for asteroseismology which is directly connected to the mean density in the star and describes the separation of consecutive radial overtones for high-order acoustic pulsation. Fig. 9 shows a schematic amplitude spectrum including all intrinsic and candidate frequencies of both MOST photometry and spectroscopy. To first view, there is no apparent equal spacing visible. If we consider the four frequencies with high S/N (solid lines) to estimate the spacing, the only reasonable solution corresponds to $f_1 - f_2 = 51$ µHz, a value already noted by Huber et al. (2008). Lower values (such as 20 or 30 µHz) although seem tempting, would however contradict the previously determined temperature and luminosity of 10 Aql (see fig. 4 in Huber et al. 2008). Assuming $\Delta \nu = 51$ µHz to be correct, Fig. 9 shows the expected position of other radial orders for three different spherical degrees ℓ (vertical dashed, dotted and dashed–dotted lines, respectively) based on the position of the four highest
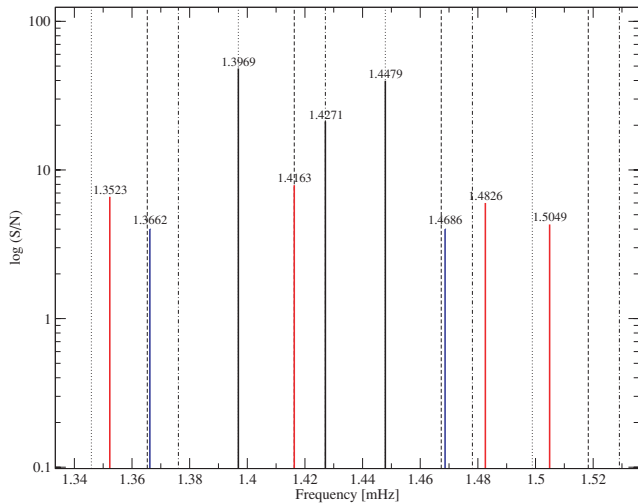
Figure 9. The observed secure (black lines) and tentative frequencies from the photometry (blue lines) and spectroscopy (red lines). The expected position of radial orders for three different spherical degrees ℓ (vertical dashed, dotted and dashed–dotted lines, respectively) is calculated based on a large separation of $f_1 - f_2 = 51\,\mu$Hz.

S/N peaks. Evidently, the agreement is not very convincing. Nevertheless, an average deviation of about 5 μHz (which is needed to align the observed values to the expected position) is about the order of the frequency shifts of consecutive radial overtones due to the magnetic field perturbation as predicted by theory (see e.g. Cunha 2006). It must be noted, however, that such suggestion can lead to (almost) any desired result and therefore have to be considered with extreme caution.

Generally, the frequencies we derived from spectroscopy do not contradict to those from MOST photometry. However, spectroscopic data provide an additional information useful for modelling. According to Huber et al. (2008) the best model describing the pulsation features in 10 Aql derived from spectroscopy corresponds to a star of $1.95\,M_\odot$, $T_{\rm eff} = 7730$ K and normal solar composition with the boundary reflection layer at $\log\tau_{5000} \sim -4$. The spectroscopic analysis reveals a pulsation node in the Nd II–Nd III line formation region. A NLTE analysis of these lines suggested that they are formed in roAp stars in atmospheric layers above $\log\tau_{5000} = -4$ (Mashonkina et al. 2005), thus indicating the position of the node. Indeed, a pulsation node is predicted at $\log\tau_{5000} = -4$ in a star of $1.95\,M_\odot$, $T_{\rm eff} = 7730$ K but assuming helium depletion (Saio, private communication), which would better correspond to the typical chemistry of a magnetic peculiar star. Therefore, combining simultaneous photometric and spectroscopic observations, we expect to improve the pulsation model of 10 Aql. This analysis will be presented in the next paper.

9.2 Interpretation of spectroscopic pulsation measurements

Here, as in many other recent studies of pulsational RV variations of roAp stars, we interpret the measurements of amplitude and phase in terms of outward propagation of pulsation waves in a chemically stratified stellar atmosphere. Previously, this interpretation of spectroscopic observations of multiperiodic roAp stars was handicapped by short spectroscopic time series which did not allow to resolve frequency patterns of multiperiodic pulsators. Here we overcome this difficulty by combining time-resolved observations acquired during several nights, but with a poor duty cycle, with a continuous

photometric monitoring by MOST at the same time. This strategy allows us to resolve the vertical structure of the three principal modes in 10 Aql and to study the propagation of pulsation waves independently for all three frequencies.

We detect a radial node in the region sampled by the formation heights of Nd and Pr for all three frequencies. The maximum amplitudes are observed for the Dy III and Tb III lines that are presumably formed below and above the region of the node. The existence of a node is supported by the bisector analysis of the Nd III 5102 Å line.

By attributing the differences in the RV curves of different REE ions to the vertical structure of oscillations we have implicitly assumed that different species sample the horizontal structure of pulsation modes in a similar manner. This might not be the case if the vertical distribution of pulsation amplitude and phase depends strongly on the stellar surface position due to a spotty element distribution combined with an intrinsic dependency of the mode structures on the orientation and strength of the magnetic field. The importance of the latter effect, arising from a superposition of magnetic and acoustic components of pulsation waves, has been recently emphasized by Sousa & Cunha (2008b).

Because of a long rotation period we are unable to constrain the surface abundance distribution of 10 Aql in the same way as it could be done for rapidly rotating roAp stars (Kochukhov 2006). For this reason it is not straightforward to distinguish between the vertical and horizontal structural effects. At the same time we see only small changes in the line profiles in a comparison of observations obtained in 2001 and 5 yr later. Furthermore, the independent evidence for a node provided by phase–amplitude diagrams and bisector analyses of different REE ions suggests that the observed phase variation corresponds rather to a vertical structure and not to a different horizontal sampling of the stellar surface.

9.3 Comparison with 33 Lib

A comparison of the pulsation properties of 33 Lib and 10 Aql is of considerable interest because these are the only roAp stars with clear signatures of a radial node in the upper atmosphere. Ryabchikova et al. (2007b) performed a pulsation analysis of 33 Lib using phase–amplitude diagrams, which enable a direct comparison of the vertical pulsation structure in two stars. The top panel of Fig. 10 displays the phase–amplitude diagram for 33 Lib, while bisector measurements of Nd III lines are compared for both stars in the lower panel of Fig. 10.

A pulsation node is clearly present in the atmospheres of both stars but the phase jump has opposite sign. Taking into account that the REE elements are concentrated in the upper atmospheric layers close to or even above the Hα line core formation zone, we can conclude from Figs 4 and 10 that the phase changes by 0.5 between the formation zones of Dy III and Tb III in the upper atmosphere of 10 Aql, while it jumps by -0.5 between Nd II and Nd III in 33 Lib.

Interestingly, the bisector measurements give us just the opposite phase variation with depth if one treats the line profile as being produced in a normal stellar atmosphere where the line core is formed higher than the line wings. As we show in the lower panel of Fig. 10, the phase decreases from the wing to the core in 10 Aql, and increases in 33 Lib. At present we do not have a definite interpretation of this discrepant behaviour. One can suspect that the broad wings of strong REE lines actually originate in the outer atmosphere and hence show pulsational characteristics of these layers.

Although the atmospheric parameters of 10 Aql and 33 Lib are similar, 33 Lib has a much stronger magnetic field, $\langle B \rangle = 5.0$ kG,
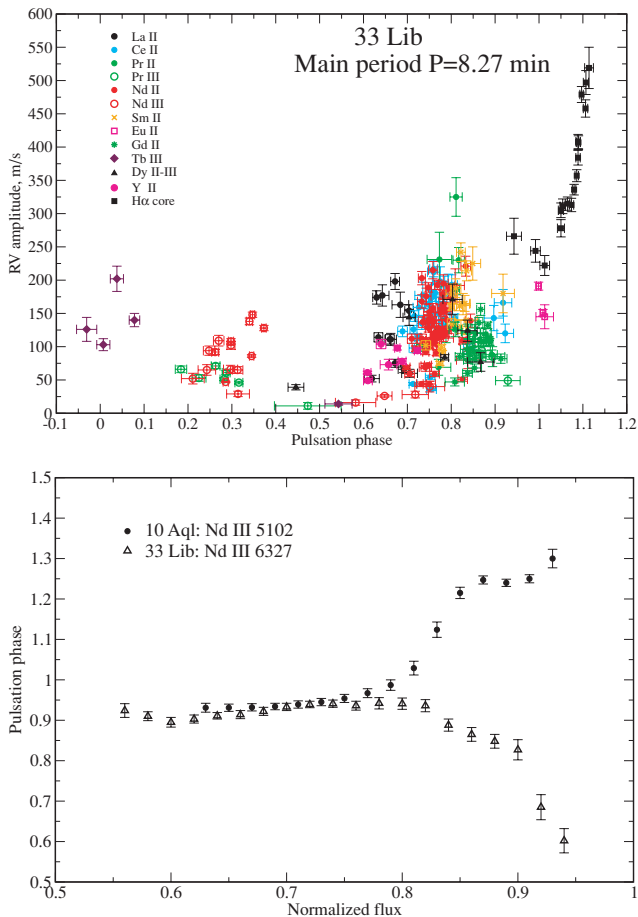
Figure 10. Amplitude–phase diagram for 33 Lib (upper panel) and pulsation phases of bisector measurements at various normalized flux levels of Nd III lines in 10 Aql and 33 Lib (lower panel). The phases are given as fractional pulsation period. For demonstration purpose the phases of 33 Lib (lower panel) are shifted by +0.6.

and it has a higher overabundance of REEs (see Ryabchikova et al. 2004). In addition, it has a shorter main pulsation period, $P = 8.27$ min, with the first harmonic exhibiting the highest amplitude close to the position of a radial node. The negative phase jump and the shape of the amplitude–phase diagram (Fig. 10, upper panel) may be interpreted as a superposition of standing and running pulsation waves mimicking an inwardly propagating wave, as discussed by Sousa & Cunha (2008b). A detailed study of chemical stratification and atmospheric structure of both stars is required for a secure interpretation of pulsation results and subsequent theoretical modelling.

9.4 Comparison with previous spectroscopic pulsation studies of 10 Aql

Non-radial pulsations in 10 Aql were investigated in four different spectroscopic observing campaigns, including the present one. Kochukhov et al. (2002) found that RV amplitudes in Eu II and Gd II lines exceed those determined for Nd III line, which was not typical for a roAp star. Additionally, Kochukhov et al. (2002) detected a change of RV amplitude between two consecutive nights of their observations. These characteristics of pulsational behaviour of 10 Aql are confirmed in the present more extensive analysis.

Hatzes & Mkrtichian (2005) observed the star during three nights, clearly detecting pulsational variability in five lines. They found the highest pulsation amplitudes of a few hundred m s^{-1} in the three spectral lines of $\lambda\lambda$5373, 5471, 5730 Å, which could not be identified. We also find significant amplitudes in these spectral features and tentatively identify these lines as Dy III, which allowed us to investigate variation of these lines in context of pulsation wave propagation through a stellar atmosphere with chemical stratification.

A recent study by Elkin et al. (2008) presented measurements of the pulsation amplitudes and phases based on UVES spectroscopic time series over 2 h, which we included in our present analysis allowing for an increase of our spectroscopic data by 10 per cent. Elkin et al. (2008) assumed that 10 Aql pulsates with a main frequency of 1.428 mHz, which is, in fact, close to one of the three main frequencies unambiguously detected in our spectroscopy and in the MOST photometry, but with the lowest amplitude. The second frequency detected by Elkin et al. (2008) at 1.309 mHz is based on variations of Tb III lines, and is not seen in our more voluminous data. It probably is an artefact caused by e.g. the limited time-span of their spectroscopic observations of this multiperiodic pulsator.

Our study is the first to resolve the frequency spectrum of 10 Aql with RV measurements. We find, in agreement with precise space photometry, that pulsations of 10 Aql are dominated by *three* modes of comparable amplitude. Based on simultaneous spectroscopic and photometric observations, we were able to infer pulsational characteristics of individual modes as a function of height in the atmosphere of 10 Aql. We also obtained phase shifts between luminosity and RV variations providing constraints for modelling of roAp pulsation.

Since our time series analysis is based on a set of three frequencies, the RV amplitudes that we report for individual lines cannot be directly compared with the results of previous studies which assumed monoperiodic variation of the star. However, a good agreement with the results by Elkin et al. (2008) is found if we compare relative amplitudes and phase differences of the spectral features in common. The two studies obtained qualitatively similar phase–amplitude diagrams, with the exception of discordant behaviour of weak Er III 5903 Å line studied by Elkin et al. (2008). The pulsation characteristics of this line deviate from the generally smooth phase–amplitude behaviour of other REE ions. We omitted this line from our pulsation analysis because it is located in the spectral region full of telluric lines and is blended by three atmospheric lines of different intensity. This blending is the most likely reason for the deviating behaviour of the spectral line Er III 5903 Å.

9.5 Amplitude modulation in spectroscopy

Time-resolved spectroscopic observations of roAp stars seemed to indicate that the pulsation amplitudes of REE lines can be modulated on a time-scale of a few hours. This was first noted by Kochukhov & Ryabchikova (2001b) for α Cir and later observed by Kurtz et al. (2006) for a few other roAp stars. Since in many cases this modulation cannot be linked to known photometric pulsation frequencies, Kurtz et al. (2006) speculated that the amplitude modulation in spectroscopy suggests the discovery of a new type of pulsational behaviour in the upper atmospheres of roAp stars. However, using relatively short and typically 2-h long time series resulting in only 100–150 individual measurements, this discovery is doubtful, because such short observational data sets do not allow to resolve the frequency spectrum of multiperiodic roAp stars. In this context it comes not as a surprise that for the only two roAp

stars, HD 24712 (Ryabchikova et al. 2007a) and 10 Aql (this paper), for which an extensive spectroscopic (and photometric) monitoring over many nights was performed, no unexplained spectroscopic amplitude modulation could be found. All amplitude modulations in 10 Aql can be explained by beating effects of close frequencies. Hence, we recommend extreme caution in the interpretation of amplitude changes seen in short data sets.

REFERENCES

Babcock H. W., 1958, ApJS, 3, 141
Belmonte J. A., Martinez Roger C., Roca Cortes T., 1991, A&A, 248, 541
Belmonte J. A., Kreidl T. J., Martinez Roger C., 1992, Inf. Bull. Var. Stars, 3752, 1
Bigot L., Dziembowski W. A., 2002, A&A, 391, 235
Cunha M. S., 2006, Mem. Soc. Astron. Ital., 77, 447
Cunha M. S., Fernandes J. M. M. B., Monteiro M. J. P. F. G., 2003, A&A, 343, 831
Elkin V. G., Kurtz D. W., Mathys G., 2008, MNRAS, 386, 481
Hatzes A. P., Mkrtichian D. E., 2005, A&A, 430, 279
Heller C. H., Kramer K. S., 1988, PASP, 100, 583
Heller C. H., Kramer K. S., 1990, MNRAS, 244, 372
Horne J. H., Baliunas S. L., 1986, ApJ, 302, 757
Huber D. et al., 2008, A&A, 483, 239
Kanaan A., Hatzes A. P., 1998, ApJ, 503, 848
Kochukhov O., 2004a, in Zverko J., Žižňovský J., Adelman S. J., Weiss W. W., eds, IAU Symp. 224, The A-Star Puzzle. Cambridge Univ. Press, Cambridge, p. 433
Kochukhov O., 2004b, ApJ, 615, L149
Kochukhov O., 2005, in Alecian G., Richard O., Vauclair S., eds, EAS Publ. Ser. Vol. 17, Element Stratification in Stars: 40 Years of Atomic Diffusion. EAS, France, p. 103
Kochukhov O., 2006, A&A, 446, 1051
Kochukhov O., 2007a, Commun. Asteroseismol., 150, 39
Kochukhov O., 2007b, in Romanyuk I. I., Kudryavtsev D. O., eds, Physics of Magnetic Stars. SAO RAS, Nizhnij Arkhyz, p. 109
Kochukhov O., Bagnulo S., 2006, A&A, 450, 763
Kochukhov O., Ryabchikova T., 2001a, A&A, 374, 615
Kochukhov O., Ryabchikova T., 2001b, A&A, 377, L22
Kochukhov O., Landstreet J. D., Ryabchikova T. A., Weiss W. W., Kupka F., 2002, MNRAS, 337, L1
Kochukhov O., Ryabchikova T., Weiss W. W., Landstreet J. D., Lyashko D., 2008, MNRAS, 376, 651
Kochukhov O., Ryabchikova T., Bagnulo S., Lo Curto G., 2008, Contrib. Astron. Obser. Skalnaté Pleso, 38, 423
Kupka F., Piskunov N., Ryabchikova T. A., Stempels H. C., Weiss W. W., 1999, A&AS, 138, 119

Kurtz D. W., 1982, Inf. Bull. Var. Stars, 1436, 1
Kurtz D. W., Martinez P., 2000, Balt. Astron., 9, 253
Kurtz D. W., Elkin V. G., Mathys G., 2005, MNRAS, 358, L6
Kurtz D. W., Elkin V. G., Mathys G., 2006, MNRAS, 370, 1274
Lenz P., Breger M., 2004, in Zverko J., Žižňovský J., Adelman S. J., Weiss W. W., eds, IAU Symp. 224, The A-Star Puzzle. Cambridge Univ. Press, Cambridge, p. 786
Leone F., Catanzaro G., 2004, A&A, 425, 271
Leone F., Vacca W. D., Stift M. J., 2003, A&A, 409, 1055
Lyashko D. A., Tsymbal V. V., Makaganuik V. A., 2007, in Mashonkina L., Sachkov M., eds, Spectroscopic Methods in Modern Astrophysics. INASAN, Moscow, p. 100
Martinez P., Sekiguchi K., Hashimoto O., 1994, MNRAS, 268, 169
Mashonkina L., Ryabchikova T., Ryabtsev A., 2005, A&A, 441, 309
Mashonkina L. et al., 2008, A&A, 478, 529
Matthews J. M., Wehlau W. H., Walker G. A. H., Yang S., 1988, ApJ, 324, 1099
Matthews J. M., Wehlau W. H., Rice J., Walker G. A. H., 1996, ApJ, 459, 278
Matthews J. M., Kurtz D. W., Martinez P., 1999, ApJ, 511, 422
Michaud G., 1978, ApJ, 220, 592
Mkrtichian D. E., Hatzes A. P., Kanaan A., 2003, MNRAS, 345, 781
Nesvacil N., Weiss W. W., Kochukhov O., 2008, Contrib. Astron. Obser. Skalnaté Pleso, 38, 329
Piskunov N. E., 1999, in Nagendra K., Stenflo J., eds, ASSL Vol. 243, 2nd International Workshop on Solar Polarization. Kluwer, Dordrecht, p. 515
Preston G. W., 1970, PASP, 82, 87
Reegan P., 2007, A&A, 467, 1353
Ryabchikova T., 2004, in Zverko J., Žižňovský J., Adelman S. J., Weiss W., eds, IAU Symp. 224, The A-Star Puzzle. Cambridge Univ. Press, Cambridge, p. 283
Ryabchikova T. A., Savanov I. S., Hatzes A. P., Weiss W. W., Handler G., 2000, A&A, 357, 981
Ryabchikova T., Nesvacil N., Weiss W. W. K. O., Stütz Ch., 2004, A&A, 423, 705
Ryabchikova T. et al., 2005, A&A, 429, L55
Ryabchikova T., Ryabtsev A., Kochukhov O., Bagnulo S., 2006, A&A, 456, 329
Ryabchikova T. et al., 2007a, A&A, 462, 1103
Ryabchikova T., Sachkov M., Kochukhov O., Lyashko D., 2007b, A&A, 473, 907
Ryabchikova T., Mashonkina L., Ryabtsev A., Kildiyarova R., Khristoforova M., 2007c, Commun. Asteroseismol., 150, 81
Ryabchikova T., Kochukhov O., Bagnulo S., 2008, A&A, 480, 811
Sachkov M. et al., 2006, Commun. Asteroseismol., 147, 97
Sachkov M., Kochukhov O., Ryabchikova T., Leone F., Bagnulo S., Weiss W. W., 2008, Contrib. Astron. Obser. Skalnaté Pleso, 38, 323
Saio H., 2005, MNRAS, 350, 1022
Saio H., Gautschy A., 2004, MNRAS, 350, 485
Savanov I. S., Malanushenko V. P., Ryabchikova T. R., 1999, Astron. Lett., 25, 802
Sousa S. G., Cunha M. S., 2008a, MNRAS, 386, 351
Sousa J. C., Cunha M. S., 2008b, Contrib. Astron. Obser. Skalnaté Pleso, 38, 453
Tsymbal V., Lyashko D., Weiss W. W., 2003, in Piskunov N., Weiss W. W., Gray D. F., eds, IAU Symp. 210, Modelling of Stellar Atmospheres. Astron. Soc. Pac., San Francisco, p. E49
Walker G. et al., 2003, PASP, 115, 1023

This paper has been typeset from a TEX/LATEX file prepared by the author.